

# 1 A 406-year non-growing season precipitation reconstruction in the 2 southeastern Tibetan Plateau

3 Maierdang Keyimu<sup>1,2</sup>, Zongshan Li<sup>1\*</sup>, Bojie Fu<sup>1</sup>, Guohua Liu<sup>1</sup>, Weiliang Chen<sup>1</sup>, Zexin Fan<sup>3</sup>, Keyan Fang<sup>4</sup>,  
4 Xiuchen Wu<sup>5</sup>, Xiaochun Wang<sup>6</sup>

5 <sup>1</sup>State Key Laboratory of Urban and Regional Ecology, Research Center for Eco-Environmental Sciences, Chinese Academy  
6 of Sciences, Beijing 100085, China

7 <sup>2</sup>Xinjiang Key Laboratory of Desert Plant Roots Ecology and Vegetation Restoration, Xinjiang Institute of Ecology and  
8 Geography, Chinese Academy of Sciences, Urumqi 830011, China

9 <sup>3</sup>Xishuangbanna Tropical Botanical Garden, Chinese Academy of Sciences, Mengla 666303, China

10 <sup>4</sup>Key Laboratory of Humid Subtropical Eco-Geographical Process (Ministry of Education), College of Geographical Sciences,  
11 Fujian Normal University, Fuzhou 350007, China

12 <sup>5</sup>State Key Laboratory of Earth Surface Processes and Resource Ecology, Beijing Normal University, Beijing 100875, China

13 <sup>6</sup>College of Forestry, Northeast Forestry University, Harbin 150040, China

14 *Correspondence to:* Zongshan Li (zsli\_st@rcees.ac.cn)

15 **Abstract.** Trees record climatic conditions during their growth, and tree rings serve as proxy to reveal the features of the  
16 historical climate of a region. In this study, we collected tree-ring cores of forest hemlock (*Tsuga forrestii*) from the  
17 northwestern Yunnan area of the southeastern Tibetan Plateau (SETP), and created a residual tree-ring width (TRW)  
18 chronology. An analysis of the relationship between tree growth and climate revealed that precipitation during the non-growing  
19 season (NGS) (from November of the previous year to February of the current year) was the most important constraining factor  
20 on the radial tree growth of forest hemlock in this region. In addition, the influence of NGS precipitation on radial tree growth  
21 was relatively uniform over time (1956–2005). Accordingly, we reconstructed the NGS precipitation over the period spanning  
22 from A.D. 1600–2005. The reconstruction accounted for 28.5% of the actual variance during the common period 1956–2005.  
23 Based on the reconstruction, NGS was extremely dry during the years A.D. 1656, 1694, 1703, 1736, 1897, 1907, 1943, 1982,  
24 and 1999. In contrast, the NGS was extremely wet during the years A.D. 1627, 1638, 1654, 1832, 1834–1835, and 1992.  
25 Similar variations of the NGS precipitation reconstruction series and Palmer Drought Severity Index (PDSI) reconstructions  
26 of early growing season from surrounding regions indicated the reliability of the present reconstruction. A comparison of the  
27 reconstruction with Climate Research Unit (CRU) gridded data revealed that our reconstruction was representative of the NGS  
28 precipitation variability of a large region in the SETP. Our study provided with the first historical NGS precipitation

29 reconstruction in the SETP which enriches the understanding of the long-term climate variability of this region. The NGS  
30 precipitation showed slightly increasing trend during the last decade which might accelerate regional forest hemlock growth.

31 **Keywords:** Tree rings; Non-growing season precipitation; Reconstruction; Southeastern Tibetan Plateau

## 32 **1 Introduction**

33 Unravelling the past climate often relies on proxy records. As a widely used proxy material, tree rings provide an opportunity  
34 to obtain long-term climate data (Fritts, 1976; Esper et al., 2002; D'Arrigo et al., 2005; Li et al., 2011; Büntgen et al., 2011,  
35 2016; Cai et al., 2014; Yang et al., 2014; Schneider et al., 2015; Wilson et al., 2016; Keyimu et al., 2021). These long-term  
36 records enable us to identify the inter-annual, decadal and multi-decal variability of historical climatic conditions. They also  
37 provide a reference to better understand the nature of current climatic conditions (warming/cooling, drying/wetting) and to  
38 project the future regional climate, as well as the dynamic response of earth processes (e.g., forest growth, glacier  
39 retreat/advance, stream flow, drought frequency, and forest fires) to climate change.

40 Being the “third pole” of the Earth, the Tibetan Plateau (TP) (average 4000 m a.s.l.) is particularly sensitive to climate change  
41 and is one of the fastest warming places in the world (Chen et al., 2020). The average decadal temperature increase at the TP  
42 is 0.33°C, which is higher than the world’s average decadal temperature increase of 0.20°C (Yan and Liu, 2014). Because of  
43 its geographical extent and position within the global circulation system, the TP plays a key role in regional and global  
44 atmospheric circulation patterns (Griessinger et al., 2017), not only affecting the mid-latitude westerlies, but also influencing  
45 the Asian monsoon circulation through its thermo-dynamical feedbacks (Duan et al., 2006; Rangwala, 2009; Wu et al., 2015).

46 There are large areas of coniferous forest distributed at high altitudes in the southeastern Tibetan Plateau (SETP). Due to  
47 their age and relative lack of disturbance they are a source of proxy material (tree rings) that can be used to reveal the past  
48 climatic conditions in this region (Bräuning and Mantwill, 2004; Fan et al., 2009; Fang et al., 2010; Li et al., 2011; Wang et  
49 al., 2015; Li and Li., 2017; Shi et al., 2017; Huang et al., 2019; Shi et al., 2019; Keyimu et al., 2021). Many  
50 dendroclimatological reconstructions of hydroclimatic variables have also been conducted in the SETP (Fan et al., 2008; Zhang  
51 et al., 2015; Wernicke et al., 2015; Griessinger et al., 2017; Li et al., 2017; He et al., 2018). However, few studies have focused  
52 on the reconstruction of precipitation history (He et al., 2012; Wernicke et al., 2015). The non-growing season (NGS) of  
53 vegetation (from November of the previous year to February of the current year) includes the winter monsoon and pre-summer  
54 monsoon seasons in the SETP, and water availability during the NGS might therefore have a constraining effect on radial tree  
55 growth (Linderholm and Chen, 2005). It is important to understand the long-term precipitation variations during the NGS to  
56 evaluate the current trend of precipitation variation and estimate its future patterns, and to determine the future responses of  
57 the forest ecosystem under the changing precipitation trend. To our knowledge, however, there have been no reports of the

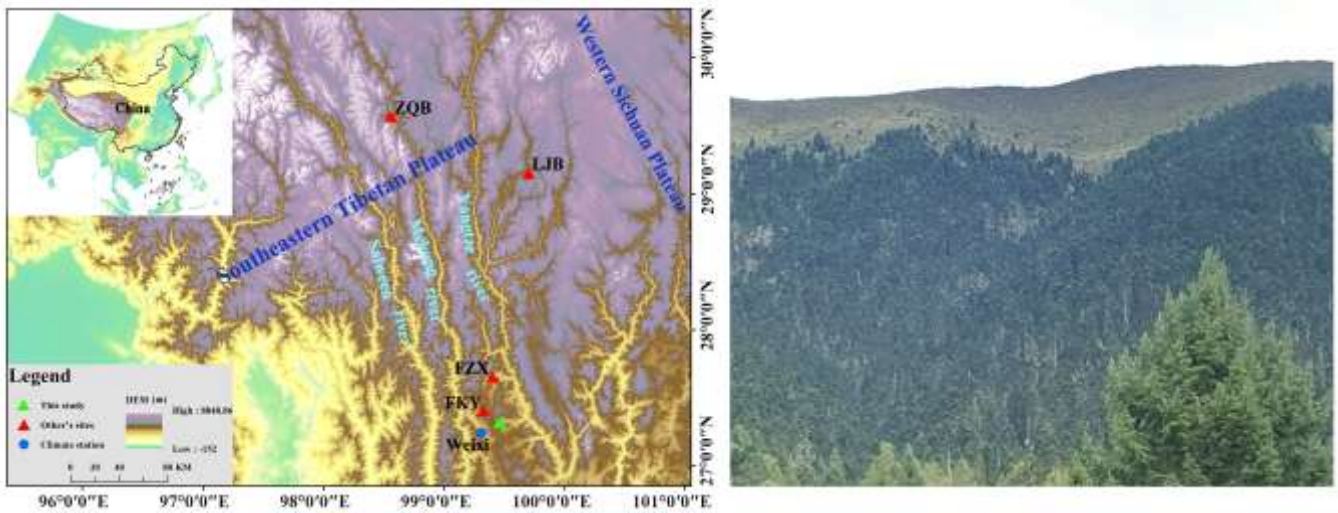
58 reconstruction of NGS precipitation in this area. This hinders our understanding of NGS variability from a long-term  
59 perspective.

60 In this study, we collected tree-ring cores of forest hemlock from the Xinzhu Village of northwestern Yunnan in the SETP.  
61 The main objectives of the present study were to (1) develop a new tree-ring chronology and identify the responses of forest  
62 hemlock radial growth to climate in the investigation area, (2) reconstruct the historical NGS precipitation and evaluate the  
63 recent NGS precipitation change in the long-term context, (3) validate the reliability of the reconstruction. Our results not only  
64 enrich the historical hydro-climatic information available in the SETP, but also provide with basis to understand the current  
65 trend of regional NGS precipitation variation, which is relevant for evaluating the future development of regional forest  
66 ecosystem.

## 67 **2 Materials and methods**

### 68 **2.1 Study area and sampling sites**

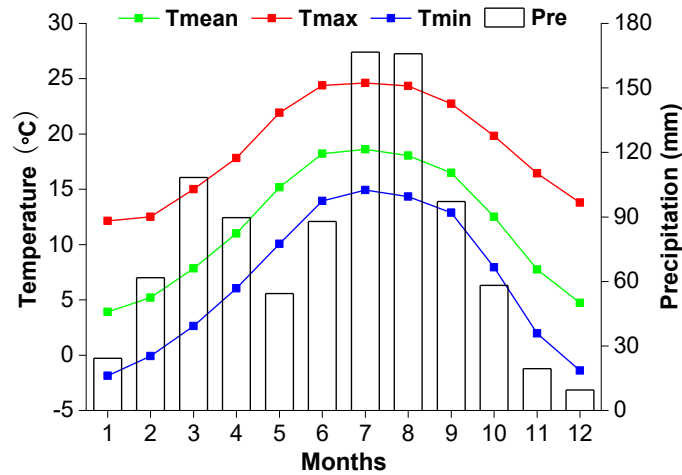
69 Tree-ring core samples were collected from Xinzhu Village in Lijiang County in northwestern Yunnan. The sample site was  
70 in the Hengduan Mountains in the SETP (Fig. 1). The climate of the study area is regulated by a westerly circulation and the  
71 monsoon circulations of the Indian and Pacific oceans. “Hengduan” means “transverse” in the Chinese language, which implies  
72 that the mountains in this region lie in the transverse direction from south to north, and the area is a passageway for the Indian  
73 monsoon to flow in and climb up to the TP and other parts of the mainland. The SETP is susceptible to monsoon flow and  
74 atmospheric circulations (Bräuning and Mantwill, 2004). According to the Weixi meteorological station of the China  
75 Meteorological Administration, which was the closest station to our sampling site, the mean annual precipitation was 953 mm  
76 from 1955 to 2016. Most of the annual precipitation (Nearly 70%) concentrated in the monsoon season from May to October  
77 in this region (Fig. 2), and thus, tree growth is usually constrained by water availability during non-growing season. The coldest  
78 temperature was  $-2.9^{\circ}\text{C}$  in January and the warmest temperature was  $18.6^{\circ}\text{C}$  in July. The topography of the sampling area is  
79 relatively steep, and it is not in favor of the soil development, hence, thin soil layer of alpine meadow soil (Chinese soil  
80 taxonomy) covers the bedrock. Forest hemlock is the dominant tree species of the sampling site, and its tree-ring cores were  
81 collected from trees which are healthy and relatively isolated, an optimal condition for maximizing climate signals in tree rings  
82 (Li et al., 2017). The elevation of the sampling site was 2,966 m a.s.l. A total of 48 tree-ring cores were extracted from 48 trees  
83 using a 5.1 mm diameter increment borer. We have used one sampling per tree method to improve the spatial representativity  
84 of radial tree growth. Sampling was conducted along an axis perpendicular to the slope inclination to avoid the impact of  
85 tension wood (Keyimu et al., 2020).



86

87 **Figure 1:** Map of the study area. The green triangle is the study site. The red triangles are the sites in other studies (previous year May –  
 88 current year April PDSI reconstruction site in Fang et al., 2010; current year March – May PDSI reconstruction site in Fan et al., 2008;  
 89 current year April – June PDSI reconstruction site in Li et al., 2017; current year May – June PDSI reconstruction site in Zhang et al., 2015).  
 90 The blue dot is the meteorological station in Weixi County. On the right is the landscape image of tree ring sampling site.

91



92

93 **Figure 2:** The ombrothermic diagram of the climate variables in the study area

94 **2.2 Establishment of the tree-ring chronology**

95 The tree-ring samples were treated with standard dendrochronological procedures. They were first glued onto wooden holders  
 96 and air-dried, and then polished to a flat surface with sand paper until the tree rings were clearly visible. The LINTAB 6.0 tree

97 ring measurement system was used to measure the tree-ring width (TRW). We have marked the tree rings of each sample at  
98 each ten-year interval and visually checked the tree ring pattern matching among samples, then confirmed the crossdating  
99 quality using the COFFECHA program (Holmes, 1983). Thirty-eight of the tree-ring cores were adopted for a further analysis  
100 after excluding the bad quality samples and the un-crossdated samples. The tree-ring series was detrended with a negative  
101 exponential model to remove the age dependency of tree growth (Cook et al., 1995). We have used the residual chronology  
102 since it removes the auto-correlation in tree ring growth and captures high frequent climate signal. The “dplR” software toolkit  
103 (Bunn, 2018) within the R software environment (R Core Team 2020) was used for detrending and chronology establishment.  
104 The reliable period of the chronology was determined based on the criterion of expressed population signal (EPS) > 0.85  
105 (Wigley, 1984).

### 106 **2.3 Climate data**

107 Temperature and precipitation records were obtained from the Weixi meteorological station (27.17° N, 99.28° E, 2326 m a.s.l.)  
108 operated by the China Meteorological Administration. Data was available for the period of 1955–2005. Climate data (including  
109 the maximum, minimum and average temperatures, and precipitation) were provided by the China Meteorological Data  
110 Sharing Service Platform. A self-calibrated Palmer Drought Severity Index (scPDSI) was downloaded from the 3.26e gridded  
111 dataset of the Climate Research Unit (CRU) via the Royal Netherlands Meteorological Institute (KNMI) climate explorer (data  
112 accessed on 23<sup>rd</sup> December, 2020, data re-accessed for the updated version (CRU scPDSI 4.05 early) of PDSI data on 20<sup>th</sup> of  
113 April, 2021) using the coordinates of the tree ring sampling site. The range of CRU grid box is 27.0 – 27.5° N, 99.0 – 99.5° E.

### 114 **2.4 Tree growth and climate relationship analysis**

115 We analysed the relationship between climate and tree growth using Dendroclim 2002 software (Biondi and Waikul, 2004).  
116 Pearson correlation values and response function values were calculated for the relationships between TRW indices and climate  
117 variables for the period of 1955–2005. Due to the carry over effect of the climatic conditions of the previous-year on the current  
118 year tree growth (Fritts, 1976), the tree growth – climate relationship analysis spanned a 16-month period from June of the  
119 previous year to September of the current year. We also used the seasonalised climate variables because it made more eco-  
120 physiological sense for growth than single months. To observe the temporal stability of the climate influence on radial tree  
121 growth, we conducted a moving correlation analysis at a moving interval of 32 years. All the correlation results were considered  
122 significant at the 95% confidence level.

### 123 **2.5 Statistics of chronology and climate reconstruction**

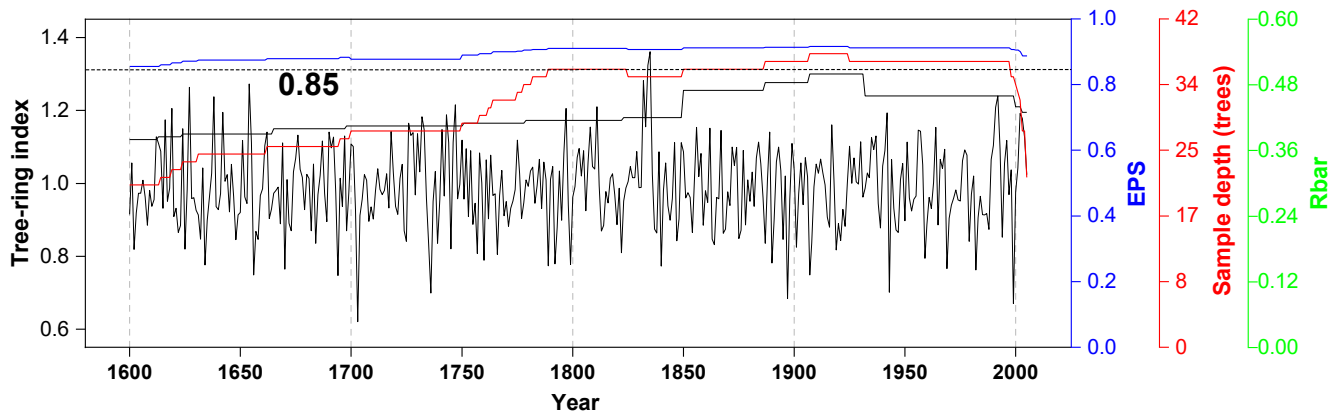
124 We have used the expressed population signal (EPS) to determine the reliable period of the chronology; mean inter-series  
125 correlation ( $\bar{R}$ ), signal-to-noise ratio (SNR) and variance of first eigenvector (VFE) to evaluate the common signal among  
126 measurement series; standard deviation (SD) and mean sensitivity (MS) to show the degree of inter-annual variability of the

127 chronology. According to the analysis of the relationship between the TRW indices and constraining climatic factors, we  
128 developed a linear regression model (Cook and Kairiukstis, 1990) for the climate reconstruction. As in many other tree ring  
129 based climate reconstructions, we tested the goodness-of-fit of the model using the leave-one-out cross-validation method  
130 (Michaelsen, 1987). We used the Pearson's correlation coefficient ( $r$ ), explained variance ( $R^2$ ), adjusted explained variance  
131 ( $R_{adj}^2$ ), reduction of error (RE), sign test (ST), coefficient of efficiency (CE), and product mean test (Pmt) to evaluate the  
132 fidelity of the reconstruction model (Fritts et al., 1990).

### 133 3. Results

#### 134 3.1 Characteristics of the TRW chronology

135 Residual TRW chronology of forest hemlock from the investigation area was established (Fig. 3). The descriptive statistics of  
136 the chronology were presented in Table 1. According to the criteria of  $EPS > 0.85$ , the most reliable length of the TRW  
137 chronology was 406 years (A.D. 1600–2005). The mean correlation among tree-ring series ( $Rbar$ ) was 0.48, and the variance  
138 in the first eigenvector (VFE) was 27 %, which implied a relatively strong common signal among individual trees constituting  
139 the chronology. The relatively low inter-annual variability of the chronology was expressed by the small mean sensitivity value  
140 (0.23). The EPS and SNR values (average EPS and SNR were 0.89 and 6.87 for the total length chronology, respectively)  
141 further implied the existence of the common signal among each individual measurement series. In general, all the statistical  
142 parameters indicated the potential climate signal imprinted in our TRW chronology.



143

144 **Figure 3:** Plot of tree-ring residual chronology, the running inter-correlations among cores ( $Rbar$ , the green line), expressed population  
145 signal (EPS, the blue line) and the sample size (the red line). The  $Rbar$  and EPS were calculated using a 30-year window, with a 15-year lag.  
146 The horizontal dashed line denotes the EPS threshold level (0.85).

147

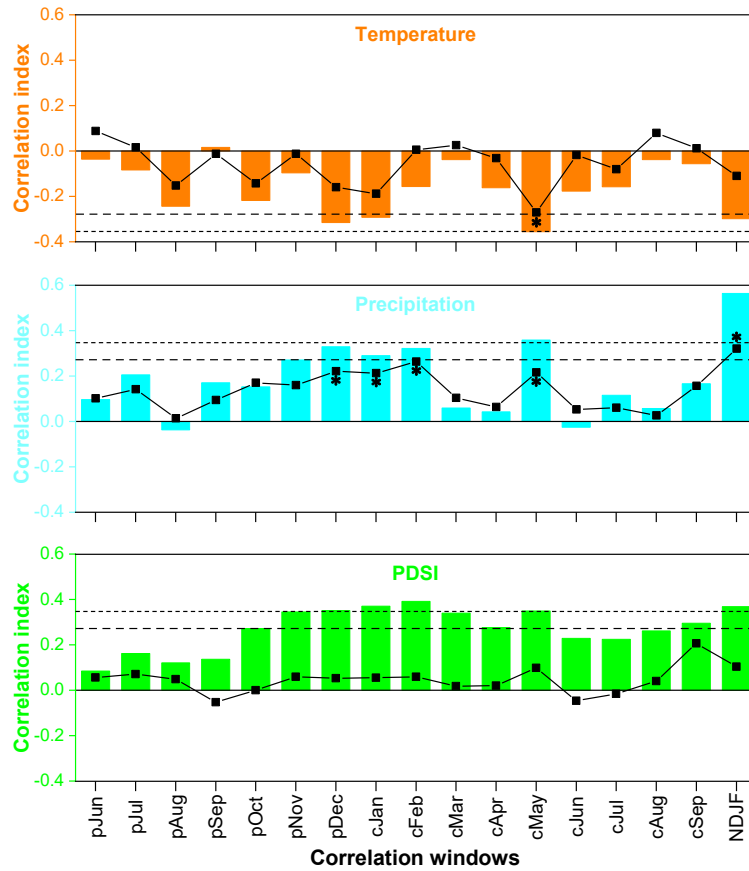
148 **Table 1. Site information, chronology statistics and results of a common interval span analysis of residual tree-ring**  
149 **width (TRW) chronology from the Xinzhu Village, northwestern Yunnan in China**

Type	Location	Elevation (m)	Time length	Number of cores	SD	MS	Rbar	SNR	EPS	VFE
Tree ring	99.43°E, 27.25°N	2966	1600–2005	38	0.22	0.23	0.48	6.87	0.89	0.27

150 Note: SD: standard deviation, MS: mean sensitivity, Rbar: mean inter-series correlation, SNR: signal-to-noise ratio, EPS: Expressed  
151 Population Signal, VFE: Variance in first eigenvector.

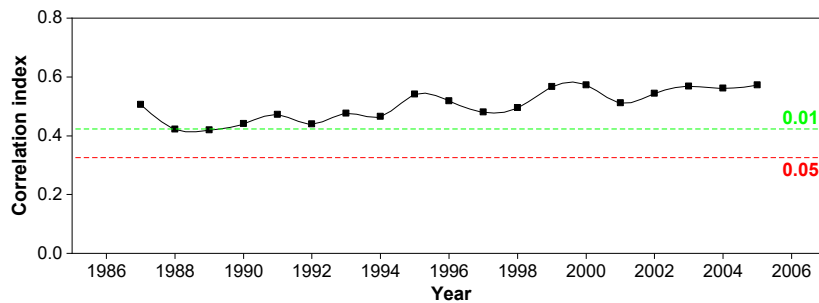
### 152 **3.2 Tree growth and climate relationship analysis**

153 According to the results of the tree growth and climate relationship analyses (Fig. 4), the precipitation during the NGS was the  
154 most important constraining factor ( $R = 0.56$ ,  $p < 0.001$ ) on the radial growth of forest hemlock in the study area. The results  
155 of a response function analysis further confirmed the strong correlation between NGS precipitation and forest hemlock radial  
156 growth. The results of a moving correlation analyses between TRW chronology and instrumental NGS precipitation record  
157 (Fig. 5) were positively significant (at 99%) during the investigated period (1956-2005), indicating that the NGS precipitation  
158 influence was stationary over time.



159

160 **Figure 4:** Correlations between tree-ring indices and temperature, precipitation, and scPDSI in the correlation windows from  
 161 previous year June to current year September, as well as in NDJF (non-growing season, NGS) for the common period from  
 162 1956 to 2005. The horizontal dashed and dotted lines indicate the threshold of the correlations at the 95% and 99% significance  
 163 levels. Black line with squares denotes the results of response function analysis between tree-ring indices and climate variables.  
 164 The asterisks next to the squares denote the significant effects ( $p < 0.05$ ) of response function analyses.



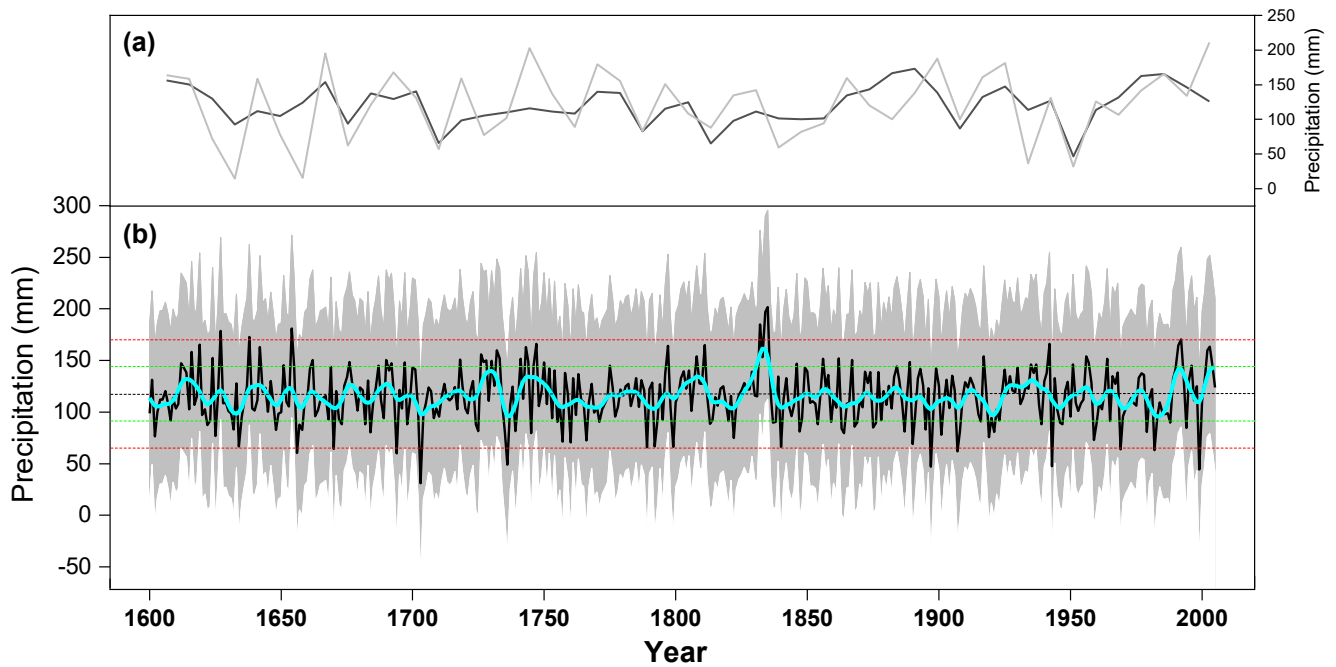
165



166 **Figure 5:** The moving correlation result between tree-ring width (TRW) chronology and non-growing season (NGS) precipitation during  
167 the period of 1956–2005. The horizontal red and green dashed lines denote the significance levels of 0.05 and 0.01, respectively.

### 168 3.3 Non-growing season precipitation reconstruction

169 According to the relationship between the TRW chronology and NGS precipitation, we developed a linear regression model  
170 ( $y = 229.94x - 109.45$  mm) and reconstructed the historical NGS precipitation series, which extended back to A.D. 1600 (Fig.  
171 6b). In the model,  $y$  is the NGS precipitation, and  $x$  is the TRW index. The reconstruction accounted for 28.5% of the  
172 instrumental NGS precipitation variability during the common time span (1956–2005). Figure 6a shows the similarities  
173 between the instrumental and reconstructed NGS precipitation series. We used a leave-one-out cross-verification method to  
174 evaluate the legitimacy of the reconstruction model (Table 2). The positive RE and CE values (0.18 and 0.15, respectively)  
175 were indicative of legitimacy of the reconstruction. The significant value (at 95%) of sign test implied that the model predicted  
176 values were generally in line with the variation trend of instrumental values. In addition, the significant values of  $F$  test (at  
177 99%) and PM test (at 95%) further confirmed the validity of the reconstruction. Overall, the statistics indicated that the  
178 reconstruction model possessed good predictive skills.



179

180 **Figure 6:** Non-growing season (NGS) precipitation reconstruction from A.D. 1600 to 2005. (a) The black line is the  
181 reconstruction series, the thick cyan line is the 11-year loess smoothed series. The horizontal black dashed line is the mean of  
182 NGS precipitation value during from A.D. 1600–2005. The horizontal green and red dashed lines are the one time and two

183 times the of standard deviations of NGS precipitation, which demonstrated the boundaries of dry and extremely dry (below  
 184 mean), and wet and extreme wet (above mean) years. The grey shading indicated the 95% confidence interval of the  
 185 reconstruction; (b) Instrumental (black) and reconstructed (grey) NGS precipitation during their common period of 1956–2005.

186 **Table 2. Leave-one-out verification statistics for the non-growing season (NGS) precipitation reconstruction**

	$R$	$R^2$	$R_{adj}^2$	$F$	Sign-test	$Pmt$	$RE$	$CE$
Calibration	0.561	0.315	0.285	–	–	–	–	–
Verification	0.524	0.274	0.235	18.6**	36+/13–*	7.89*	0.18	0.15

187 Note:  $R$  correlation coefficient,  $R^2$  explained variance,  $R_{adj}^2$  is the adjusted explained variance,  $F$   $F$ -test, Sign-test sign of paired observed  
 188 and estimated departures from their mean on the basis of the number of agreements/disagreements,  $Pmt$  product mean test,  $RE$  reduction of  
 189 error,  $CE$  coefficient of efficiency. \*  $p < 0.05$ , \*\*  $p < 0.01$

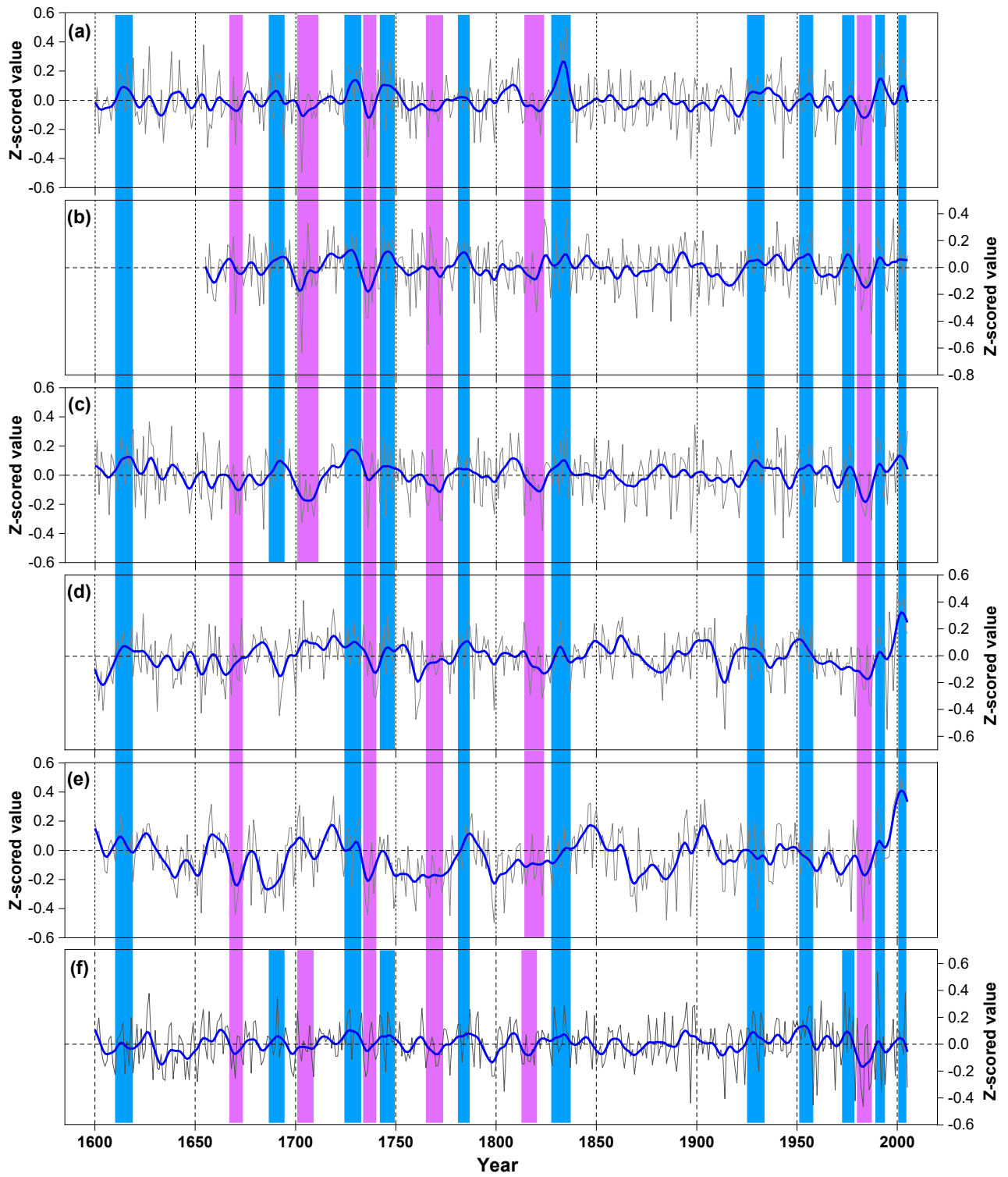
### 190 3.4 Characteristics of the NGS precipitation reconstruction

191 Figure 6b shows the reconstructed NGS precipitation over the past 406 years (A.D. 1600–2005). The mean of the reconstructed  
 192 NGS precipitation series was 118 mm, and the standard deviation (SD) was 26 mm. We pre-defined the years that had NGS  
 193 precipitation above 144 mm (mean+SD) as wet NGS years, and above 170 mm (mean+2SD) as extremely wet years (Table  
 194 3), whereas we defined years that had precipitation below 92 mm (mean-SD) as dry NGS years, and below 66 mm (mean-2SD)  
 195 as extremely dry NGS years (Table 3). The dry/wet periods and some of the extreme dry/wet NGS periods in the present  
 196 reconstruction were synchronised with dry/wet periods and extreme dry/wet periods in previously reported PDSI  
 197 reconstruction from the surrounding region (Fig. 7, Table S2, Table S3), though some dissimilarities were also existed. As  
 198 shown in Fig. 8, the instrumental (a, c) and reconstructed (b, d) NGS precipitation series could represent the climatic conditions  
 199 over a similar area in the SETP.

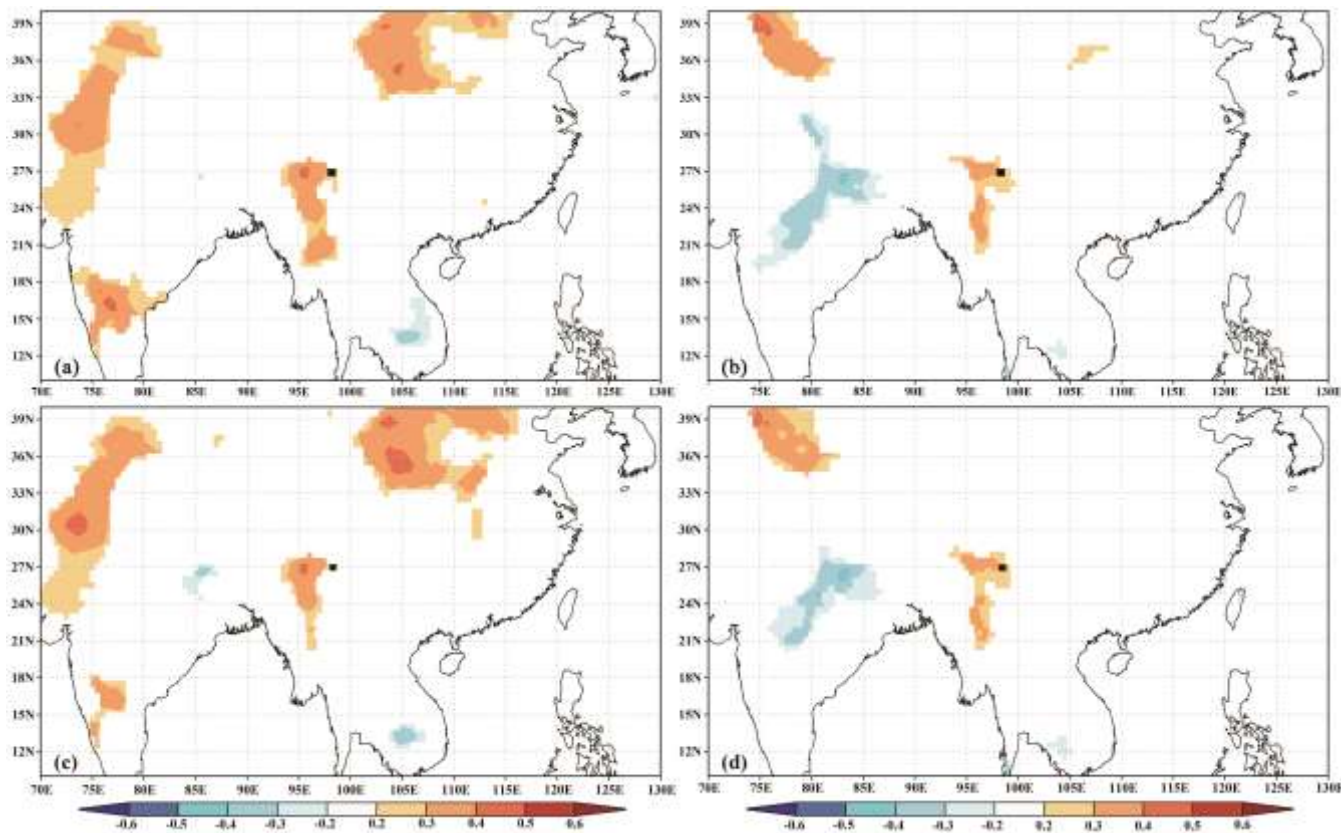
200

**Table 3 Extreme wet and dry NGS years**

Year	Dry (mm)	Year	Wet (mm)
1656	63	1627	181
1694	62	1638	175
1703	33	1654	183
1736	51	1832	187
1897	49	1834	199
1907	64	1835	204
1943	50	1992	173
1982	65		
1999	47		



202 **Figure 7:** Comparisons of the hydroclimatic reconstructions in different studies. (a) The non-growing season (NGS)  
203 precipitation reconstruction in the present study. (b) The current year March – May average Palmer Drought Severity Index  
204 (PDSI) reconstruction in Fan et al. (2008). (c) The reconstruction of average PDSI from May of the previous year to April of  
205 the current year in Fang et al. (2010). (d) The current year May-June average PDSI reconstruction in Zhang et al. (2015). (e)  
206 The current year April-June average PDSI reconstruction in Li et al. (2017). (f) drought series extracted from Asian Monsoon  
207 Atlas from the nearest point (Cook et al. 2010). The blue and purple bars show the common wet and dry periods of the different  
208 reconstructions, respectively.



209

210 **Figure 8:** Spatial correlations of actual (a: raw data; c: first-differenced data) and reconstructed (b: raw data; d: first-differenced  
211 data) non-growing season (NGS) precipitation with a gridded dataset of the NGS precipitation (average from November of the  
212 previous year to February of the current year) during their overlapping periods (1956–2005). The black square indicates the  
213 location of the study site.

## 214 4. Discussion

### 215 4.1 Tree growth and climate relationship

216 The results of the tree growth and climate relationship analyses suggested that the forest hemlock radial growth in the  
217 northwestern Yunnan region of the SETP was strongly constrained by hydroclimatic factors. According to the Pearson  
218 correlation analysis, the influence of precipitation during the NGS on radial tree growth was greater than that of any other  
219 investigated climate variables and any correlation window. The response function analysis further confirmed the strong impact  
220 of NGS precipitation. In addition, the results of 32-year interval of moving correlation analysis (Fig. 5) suggested the  
221 temporally consistent influence of NGS precipitation on forest hemlock radial growth in this region. The importance of NGS  
222 precipitation on the radial tree growth could be attributed to the fact that precipitation during the NGS compensated for the  
223 soil moisture, which was crucially important for supporting tree growth in the following season (Linderholm and Chen, 2005;  
224 Treydte et al. 2006; Wu et al., 2019; Li et al., 2021). This is because tree growth is often water stressed in the early stages of  
225 its growth in each year on the SETP when the monsoon precipitation does not arrive (Bräuning and Mantwill, 2004; Zhang et  
226 al., 2015), and the earlywood of tree rings mainly use spring melt water (Zhu et al., 2021). The eco-physiological importance  
227 of NGS precipitation on tree growth and tree water usage was also revealed by isotope ratios method-based investigations.  
228 Brinkmann et al's (2018) study showed that nearly 40% of the uptaken water by *Fagus sylvatica* and *Picea abies* trees in a  
229 temperate forest of middle Europe are sourced from NGS precipitation. Tree-ring oxygen isotope ratios ( $\delta^{18}\text{O}$ ) are  
230 demonstrated to contain NGS precipitation signals in the Himalayan region (Huang et al., 2019; Zhu et al., 2021). Huang et  
231 al's (2019) study revealed that NGS precipitation (snowfall) increased the snow-depth and the later snowmelt compensated  
232 soil moisture in the spring and early summer, which was a crucially important water source for the Juniper growth in the  
233 southwestern Tibetan Plateau. Zhu et al's (2021) investigation in the western Himalaya revealed that formation of earlywood  
234 in tree rings of *Pinus wallachina* depended on the snowmelt originated from NGS precipitation. The weak influence of  
235 precipitation on regional forest hemlock growth during March and April and strong influence during May was connected with  
236 the saddle-shaped monthly rainfall pattern of this area (Fig. 2). The highest correlation between precipitation and TRW  
237 chronology was observed in May of the current year. This is because the xylogenous activity to form earlywood coincided  
238 with the low precipitation in this month (Fig. 2). In addition, the melt water was probably used up (tree uptake + evaporation)  
239 during the early spring. Therefore, water stressed was increased during the late spring (May). The correlations between  
240 precipitation and the TRW chronology were not significant during the growing season (June-September) because an adequate  
241 water supply was available in the summer monsoon season.

242 Precipitation during the NGS over the SETP falls as snow. According to Sommerfeld et al. (1993) and Stadler et al. (1996),  
243 the development of a snowpack insulates the underlying soil from freezing temperatures, which creates unfrozen soil  
244 conditions and most of the soil processes that are active during warmer conditions also persist under snow cover, albeit at a  
245 reduced rate (Edwards, 2007). Unfrozen soil can reduce the cold and frost damage to the shallow root systems of conifer trees

246 in this region (Schenk and Jackson, 2002). A reduction in the cold damage to roots decreases the energy required to form new  
247 roots in the following growth year (Pederson et al., 2004), with the saved energy potentially used to initiate xylogenesis and  
248 form earlywood cells. Evergreen tree species are known to carry out year-round photosynthetic activity (Oquist and Huner,  
249 2003; Prats and Brodersen, 2020), albeit at a slower rate during the NGS, and therefore, the higher moisture availability  
250 contributes to the carbohydrate and energy accumulation process of forest hemlock in the investigation area.

251 In contrast, the radial tree growth was negatively correlated to temperature in most correlation windows (Fig. 4). This can  
252 be explained by the fact that higher temperature enhances evapotranspiration, and thus decreases water availability, which  
253 eventually constrains tree growth. The negative impact of NGS temperature on radial tree growth was obvious because the  
254 strengthened evaporation due to higher temperatures might reduce the moisture compensation to the soil layer and cause water  
255 stress during the early stage of the following growth season.

#### 256 **4.2 Validity of the reconstructed precipitation series**

257 We have tried to validate the fidelity of the newly reconstructed series from different aspects. Although we used the residual  
258 TRW chronology in the present study, which removes autocorrelation (Cook and Kairiukstis, 1990) to capture the high  
259 frequency climate signals as in Fan et al. (2008) and Chen et al. (2016), the variability of dry and wet NGS at different scales  
260 was still retained in the reconstructed series. The reconstructed series in the present study demonstrated the variation in dry  
261 and wet NGS years (Fig. 6b). As in many other proxy based historical climate reconstruction studies, we compared our NGS  
262 precipitation series with other hydroclimatic reconstructions from the surrounding areas to investigate the reliability of our  
263 reconstruction. However, there was no reported historical NGS precipitation record in the SETP, and we had to compare the  
264 present reconstruction series with available hydro-climatic reconstructions, e.g., PDSI. There are only countable numbers of  
265 PDSI reconstructions in the nearby region. Hence, we could only compare the present NGS precipitation reconstruction with  
266 existing PDSI reconstructions (Fig. 7) which are of spring or early summer. Dry/wet climate during these seasons are usually  
267 associated with the winter precipitation, hence, it makes certain sense to carry out the comparison. The correlation coefficients  
268 between our NGS precipitation reconstruction and the PDSI reconstructions of Fan et al. (2008), Fang et al. (2010), Zhang et  
269 al. (2015) and Li et al. (2017) were 0.51 ( $n = 702$ ), 0.35 ( $n = 1062$ ), 0.25 ( $n = 1062$ ) and 0.22 ( $n = 1016$ ) ( $p < 0.001$ ). We have  
270 extracted the drought series of Asian Monsoon Atlas (Cook et al. 2010) from the nearest point to our investigation site and  
271 compared it with the NGS precipitation reconstruction in present study ( $R = 0.35$ ,  $n = 1062$ ,  $p < 0.001$ ). As can be observed  
272 from Fig. 7, there were dry and wet periods in compared reconstruction series which were consistent with the NGS precipitation  
273 variabilities. These similarities indicated the reliability of our NGS precipitation reconstruction to some extent. The correlation  
274 coefficients for the present reconstruction with those of Fan et al. (2008) and Fang et al. (2010) were greater than those with  
275 Li et al. (2017) and Zhang et al. (2015). These differences were probably due to the different distances among the study sites.  
276 Although, the major dry and wet periods were similar in the hydroclimatic reconstructions referenced above, there were still  
277 certain discrepancies in duration and the strength of the dry/wet climatic conditions. This is probably because of the differences

278 in the types of hydroclimatic variables (precipitation, PDSI), specific seasons reconstructed (annual, seasonal), tree species  
279 (species with different drought tolerances), chronology recording methods (standard chronology, residual chronology), length  
280 of calibration period, sample replication and the geomorphic differences of the tree ring sampling sites (altitude, slope) (Table  
281 S1).

282 In addition, we uploaded both of the instrumental and reconstructed NGS precipitation data for the same period of 1956–  
283 2005 on the KNMI website and conducted a spatial correlation analysis with the CRU gridded climate dataset. The similar  
284 patterns of spatial correlation between the instrumental and reconstructed data and their first differenced data (Fig. 8) indicated  
285 that the present reconstruction was reliable and could represent the NGS precipitation over a large area in the SETP. Besides,  
286 the occurrence of some historical great drought events in the Asian monsoon area (Cook et al., 2010, Kang et al., 2013), i.e.,  
287 the 1756–1768 (strange parallels drought), 1790, 1792–1796 (east India drought) and 1920s (China mega-drought), matched  
288 the dry NGS periods in our reconstruction, which also further confirmed the reliability of our reconstruction.

## 289 **5. Conclusion**

290 In this study, we investigated 406 years of residual TRW chronology of forest hemlock in the SETP, China. The climate and  
291 tree growth relationship analyses showed that the TRW chronology was mostly negatively correlated with the thermal variable  
292 (temperature), whereas it was positively correlated with hydroclimatic variables (precipitation) and PDSI, indicating that  
293 hydroclimatic conditions determined the radial growth of forest hemlock in this region. Accordingly, we derived a linear model  
294 of the relationship between climate and tree growth, which accounted for 28.5% of the actual NGS precipitation variance  
295 (1956–2005), and we used the model to reconstruct the historical (A.D. 1600–2005) NGS precipitation. The reconstructed  
296 series showed that the NGS was extremely dry during the years A.D. 1656, 1694, 1703, 1736, 1897, 1907, 1943, 1982 and  
297 1999. In contrast, the NGS was extremely wet during the years A.D. 1627, 1638, 1654, 1832, 1834–1835 and 1992. A  
298 comparison between the NGS precipitation reconstruction in this study and PDSI reconstructions from nearby regions revealed  
299 a coherency in the timing of dry and wet episodes, suggesting the reliability of our reconstruction. Our results showed that the  
300 NGS precipitation demonstrated slightly increasing trend since 1980s which is in favor of the future forest ecosystem  
301 development. In the future, more efforts should be made to collect wide-area of tree-ring data and develop more proxy  
302 chronologies that will enable us to reveal historical precipitation variability at the longer and wider scale in the SETP.

303 **Data availability.** The climate reconstruction series in this study can be obtained from Zongshan Li after the paper publication.

304 **Author contributions.** ZSL and MK conceived the study; ZSL, ZXF, XCW collected the tree-ring data; MK, ZSL, ZXF, KYF,  
305 XCW elaborated the methodology; MK, ZSL, WLC analysed the data; MK, ZSL led the writing of the manuscript; ZSL and  
306 ZXF revised the manuscript; BJF and GHL validated the final manuscript.

307 **Competing interests.** The authors declare that they have no conflict of interest.

308 **Acknowledgement.** This work was funded by the National Key Research Development Program of China (2016YFC0502105),  
309 the second Tibetan Plateau Scientific Expedition and Research (STEP) Program (2019QZKK0502). We are grateful to the  
310 editor and anonymous reviewers for their valuable comments and suggestions to improve this article.

## 311 **References**

312 Biondi, F. and Waikul, K.: DENDROCLIM2002: a C++ program for statistical calibration of climate signals in tree ring  
313 chronologies, *Comput. Geosci.*, 30(3), 303-311, <https://doi.org/10.1016/j.cageo.2003.11.004>, 2004

314 Bräuning, A. and Mantwill, B.: Summer temperature and summer monsoon history on the Tibetan Plateau during the last 400  
315 years recorded by tree rings, *Geophys. Res. Lett.*, 31, L24205, <https://doi.org/10.1029/2004GL020793>, 2004

316 Bunn, A. G. and Korpela, M.: An introduction to dplR. The Comprehensive R Archive Network,  
317 <https://cran.biodisk.org/web/packages/dplR/vignettes/intro-dplR.pdf>, 2018

318 Büntgen, U., Myglan, V. S., Ljungqvist, F. C., McCormick, M., Di Cosmo N., Sigl, M., Jungclaus, J., Wagner, S., Krusic, P.  
319 J., Esper, J., Kaplan, J. O., de Vaan MAC., Luterbacher, J., Wacker, L., Tegel, W. and Kirdyanov, A. V.: Cooling and societal  
320 change during the Late Antique Little Ice Age from 536 to around 660 AD, *Nat. Geosci.*, 9, 231–236,  
321 <https://doi.org/10.1038/ngeo2652>, 2016

322 Büntgen, U., Tegel, W., Nicolussi, K., McCormick, M., Frank, D., Trouet, V., Kaplan, J. O., Herzig, F., Heussner, K. U.,  
323 Wanner, H., Luterbacher, J. and Esper, J.: 2500 years of European climate variability and human susceptibility, *Science*, 331,  
324 578–582, <https://doi.org/10.1126/science.1197175>, 2011

325 Cai, Q. F., Liu, Y., Lei, Y., Bao, G. and Sun, B.: Reconstruction of the march-august PDSI since 1703 AD based on tree rings  
326 of Chinese pine (*Pinus tabulaeformis* Carr.) in the Lingkong Mountain, southeast Chinese loess Plateau, *Clim. Past.*, 10, 509–  
327 521, <https://doi.org/10.5194/cp-10-509-2014>, 2014

328 Chen, F., Yuan, Y. J., Zhang, T. W., Shang, H.: Precipitation reconstruction for the northwestern Chinese Altay since 1760  
329 indicates the drought signals of the northern part of inner Asia, *Int. J. Biometeorol.*, 60(3), 455-463.  
330 <https://doi.org/10.1007/s00484-015-1043-5>, 2016

331 Cook, E. R. and Kairiukstis, A.: *Methods of Dendrochronology: Applications in the Environmental Sciences*, Kluwer  
332 Academic Press, Dordrecht, 1990

333 Cook, E. R., Anchukaitis, K. J., Buckley, B. M., D'Arrigo, R. D., Jacoby, G. C. and Wright, W. E.: Asian monsoon failure and  
334 megadrought during the last millennium, *Science*, 328(5977), 486-489, <https://doi.org/10.1126/science.1185188>, 2010

335 Cook, E. R., Briffa, K. R., Meko, D. M., Graybill, D. A. and Funkhouser, G.: The 'segment length curse' in long tree-ring  
336 chronology development for palaeoclimatic studies, *Holocene*, 5(2), 229-237. <https://doi.org/10.1177/095968369500500211>,  
337 1995



338 D'Arrigo, R. D., Mashig, E., Frank, D. C., Wilson, R. J. S. and Jacoby, G. C.: Temperature variability over the past millennium  
339 inferred from Northwestern Alaska tree rings, *Clim. Dynam.*, 24, 227-236. <https://doi.org/10.1007/s00382-004-0502-1>, 2005

340 Duan, K., Yao, T. and Thompson, L.: Response of monsoon precipitation in the Himalayas to global warming, *J. Geophys.*  
341 *Res.*, 111, D19110. <https://doi.org/10.1029/2006JD007084>, 2006

342 Edwards, A. C., Scalenghe, R., Freppaz, M.: Changes in the seasonal snow cover of alpine regions and its effect on soil  
343 processes: a review. *Quat. Int.*, 162-163, 172-181. <https://doi.org/10.1016/j.quaint.2006.10.027>, 2007

344 Esper, J.: 1300 years of climatic history for Western Central Asia inferred from tree rings, *Holocene*, 12(3), 267-277.  
345 <https://org.doi.10.1191/0959683602hl543rp>, 2002

346 Fan, Z. X., Bräuning, A. and Cao, K. F.: Tree-ring based drought reconstruction in the central Hengduan Mountains region  
347 (China) since AD 1655, *Int. J. Climatol.*, 28, 1879–1887, <https://doi.org/10.1002/joc.1689>, 2008

348 Fan, Z. X., Bräuning, A., Yang, B. and Cao, K. F.: Tree ring density-based summer temperature reconstruction for the central  
349 Hengduan Mountains in southern China, *Glob. Planet. Change*, 65 (1-2), 1-11. <https://doi.org/10.1016/j.gloplacha.2008.10.001>,  
350 2009

351 Fang, K. Y, Gou, X. H, Chen, F., Li, J. B., D'Arrigo, R., Cook, E. D, Yang, T. and Davi, N.: Reconstructed droughts for the  
352 southeastern Tibetan Plateau over the past 568 years and its linkages to the Pacific and Atlantic Ocean climate variability,  
353 *Clim. Dyn.*, 35(4), 577–585. <https://doi.org/10.1007/s00382-009-0636-2>, 2010

354 Fritts, H. C., Guiot, J. and Gordon, G. A.: Verification. In: Cook E and Kairiukstis LA, eds., *Methods of Dendrochronology:*  
355 *Applications in the Environmental Sciences*. Dordrecht, Kluwer Academic Publishers, 178-184, 1990

356 Fritts, H. C.: *Tree rings and climate*. Academic Press, London, 1976

357 Griessinger, J., Bräuning, A., Helle, G., Hochreuther, P. and Schleser, G.: Late Holocene relative humidity history on the  
358 southeastern Tibetan plateau inferred from a tree ring  $\delta^{18}\text{O}$  record: recent decrease and conditions during the last 1500 years,  
359 *Quat. Int.*, 430, 52–59, <http://dx.doi.org/10.1016/j.quaint.2016.02.011>, 2017

360 He, H. M., Bräuning, A., Griessinger, J., Hochreuther, P. and Wernicke, J.: May–June drought reconstruction over the past  
361 821 years on the southcentral Tibetan Plateau derived from tree-ring width series, *Dendrochronologia*, 47, 48–57,  
362 <https://doi.org/10.1016/j.dendro.2017.12.006>, 2018

363 He, H. M., Yang, B., Bräuning, A., Wang, J. L. and Wang, Z. Y.: Tree-ring derived millennial precipitation record for the  
364 south-central Tibetan plateau and its possible driving mechanism, *Holocene*, 23 (1), 36-45,  
365 <https://doi.org/10.1177/0959683612450198>, 2012

366 Holmes, R. L.: Computer-assisted quality control in tree-ring dating and measurement, *Tree-ring Bulletin*, 43, 69-75, 1983

367 Huang, R., Zhu, H. F., Liang, E. Y., Liu, B., Shi, J. F., Zhang, R. B., Yuan, Y. J., Griessinger, J.: A tree ring-based winter  
368 temperature reconstruction for the southeastern Tibetan Plateau since 1340 CE, *Clim. Dyn.*, 53, 3221-3233.  
369 <https://doi.org/10.1007/s00382-019-04695-3>, 2019

370 Kang, S. Y., Bao, Y., Qin, C., Wang, J. L., Feng, S., Liu, J. J.: Extreme drought events in the years 1877–1878, and 1928, in  
371 the southeast Qilian mountains and the air–sea coupling system. *Quat. Int.*, 283(427), 85-92.  
372 <https://doi.org/10.1016/j.quaint.2012.03.011>, 2013

373 Keyimu, M., Li, Z. S., Liu, G. H., Fu, B. J., Fan, Z. X., Wang, X. C. Zhang, Y. D., Halik, U.: Tree-ring based minimum  
374 temperature reconstruction on the southeastern Tibetan Plateau, *Quat. Sci. Rev.*, 251, 106712.  
375 <https://doi.org/10.1016/j.quascirev.2020.106712>, 2021

376 Keyimu, M., Wei, J. S., Zhang, Y. X., Zhang, S., Li, Z. S., Ma, K. M., Fu, B. J.: Climate signal shift under the influence of  
377 prevailing climate warming – Evidence from *Quercus liaotungensis* on Dongling Mountain, Beijing, China,  
378 *Dendrochronologia*, 60, 125683. <https://doi.org/10.1016/j.dendro.2020.125683>, 2020

379 Li, J. B., Shi, J. F., Zhang, D. D., Yang, B., Fang, K. Y. and Yue, P. H.: Moisture increase in response to high-altitude warming  
380 evidenced by tree-rings on the southeastern Tibetan Plateau, *Clim. Dyn.*, 48, 649–660. [https://doi.org/10.1007/s00382-016-](https://doi.org/10.1007/s00382-016-3101-z)  
381 [3101-z](https://doi.org/10.1007/s00382-016-3101-z), 2017

382 Li, T., Li, J.B.: A 564-year annual minimum temperature reconstruction for the east central Tibetan Plateau from tree rings,  
383 *Glob. Planet. Change*, 157, 165-173. <https://doi.org/10.1016/j.gloplacha.2017.08.018>, 2017.

384 Li, Z. S., Zhang, Q. B. and Ma, K. P.: Tree-ring reconstruction of summer temperature for A.D. 1475–2003 in the central  
385 Hengduan Mountains, northwestern Yunnan, China, *Clim. Change*, 110(1-2), 455-467, [https://doi.org/10.1007/s10584-011-](https://doi.org/10.1007/s10584-011-0111-z)  
386 [0111-z](https://doi.org/10.1007/s10584-011-0111-z), 2011

387 Linderholm, H. W., Chen, D.: Central Scandinavian winter precipitation variability during the past five centuries reconstructed  
388 from *Pinus sylvestris* tree rings, *Boreas*, 34, 43–52, <https://doi.org/10.1080/03009480510012845>, 2005

389 Michaelsen, J.: Crossevalidation in statistical climate forecast models, *J Clim. App. Meteorol.*, 26, 1589-1600, 1987

390 R: A language and environment for statistical computing. R Foundation for Statistical Computing, Vienna, Austria. URL  
391 <https://www.R-project.org/>, 2020

392 Oquist, G., Huner, N. P.: Photosynthesis of overwintering evergreen plants, *Annu. Rev. Plant Biol.*, 54, 329–355.  
393 <https://doi.org/10.1146/annurev.arplant.54.072402.115741>, 2003

394 Prats, K. A., Brodersen, C. R.: Seasonal coordination of leaf hydraulics and gas exchange in a wintergreen fern, *AoB Plants*,  
395 12(6), 1–13. <https://doi.org/10.1093/aobpla/plaa048>, 2020

396 Pederson, N., Cook, E. R., Jacoby, G. C., Peteet, D. M., Griffin, K. L.: The influence of winter temperatures on the annual  
397 radial growth of six northern range margin tree species, *Dendrochronologia*, 22 (1), 7–29.  
398 <https://doi.org/10.1016/j.dendro.2004.09.005>, 2004

399 Rangwala, I., Miller, J. R. and Xu, M.: Warming in the Tibetan Plateau: Possible influences of the changes in surface water  
400 vapor, *Geophys. Res. Lett.*, 36, L06703, <https://doi.org/10.1029/2009GL037245>, 2009

401 Schenk, H. J., & Jackson, R. B.: The global biogeography of roots. *Ecol. Monogr.*, 72, 311–328. [https://doi.org/10.1890/0012-9615\(2002\)072\[0311:TGBOR\]2.0.CO;2](https://doi.org/10.1890/0012-9615(2002)072[0311:TGBOR]2.0.CO;2), 2002

403 Schneider, L., Smerdon, J. E., Büntgen, U., Wilson, R. J. S., Myglan, V. S., Kirilyanov, A. V. and Esper, J.: Revising mid-  
404 latitude summer temperatures back to AD 600 based on a wood density network, *Geophys. Res. Lett.*, 42, 4556-4562.  
405 <https://doi.org/10.1002/2015GL063956>, 2015

406 Shi, C. M., Sun, C., Wu, G. C., Wu, X. C., Chen, D. L., Masson-Delmotte, V., Li, J. P., Xue, J. Q., Li, Z. S., Ji, D. Y., Zhang,  
407 J., Fan, Z. X., Shen, M. G., Shu, L. F., Ciais, P.: Summer temperature over Tibetan Plateau modulated by Atlantic multi-  
408 decadal variability, *J. Clim.*, 32, 4055-4067. <https://doi.org/10.1175/JCLI-D-17-0858.1>, 2019

409 Shi, S. Y., Li, J. B., Shi, J. F., Zhao, Y. S. and Huang, G.: Three centuries of winter temperature change on the southeastern  
410 Tibetan plateau and its relationship with the Atlantic Multidecadal Oscillation, *Clim. Dyn.*, 49, 1305-1319.  
411 <https://doi.org/10.1007/s00382-016-3381-3>, 2017

412 Sommerfeld, R. A., Mosier, A. R., Musselman, R. C.: CO<sub>2</sub>, CH<sub>4</sub> and N<sub>2</sub>O flux through a Wyoming snowpack and implications  
413 for global budget, *Nature*, 361, 140–142, <https://doi.org/10.1038/361140a0>, 1993

414 Stadler, D., Wunderli, H., Auckenthaler, A., Fluhler, H.: Measurement of frost induced snowmelt runoff in a forest soil, *Hydrol.*  
415 *Process.*, 10, 1293–1304, [https://doi.org/10.1002/\(SICI\)1099-1085\(199610\)10:10<1293::AID-HYP461>3.0.CO;2-I](https://doi.org/10.1002/(SICI)1099-1085(199610)10:10<1293::AID-HYP461>3.0.CO;2-I), 1996

416 Wang, J. L., Yang, B., Ljungqvist, F. C.: A millennial summer temperature reconstruction for the eastern Tibetan Plateau from  
417 tree-ring width, *J. Clim.*, 28(13), 5289-5304. <https://doi.org/10.1175/JCLI-D-14-00738.1>, 2015

418 Wernicke, J., Griessinger, J., Hochreuther, P., Bräuning, A.: Variability of summer humidity during the past 800 years on the  
419 eastern Tibetan plateau inferred from  $\delta^{18}\text{O}$  of tree-ring cellulose. *Clim. Past*, 10(4), 3327-3356. <https://doi.org/10.5194/cp-11-327-2015>. 2015

421 Wigley, T. M., Briffa, K. R., and Jones, P. D.: On the average value of correlated time series, with applications in  
422 dendroclimatology and hydrometeorology, *J. Clim. Appl. Meteorol.*, 23, 201–213, [https://doi.org/10.1175/1520-0450\(1984\)0232.0.CO;2](https://doi.org/10.1175/1520-0450(1984)0232.0.CO;2), 1984

424 Wilson, R., Anchukaitis, K., Briffa, K. R., Büntgen, U., Cook, E., D'Arrigo, R., Davi, N., Esper, J., Frank, D., Gunnarson, B.,  
425 Hegerl, G., Helama, S., Klesse, S., Krusic, P.J., Linderholm, H.W., Myglan, V., Osborn, T.J., Rydval, M., Schneider, L.,

426 Schurer, A., Wiles, G., Zhang, P. and Zorita, E.: Last millennium northern hemisphere summer temperatures from tree rings:  
427 Part I: the long-term context, *Quat. Sci. Rev.*, 134, 1-18. <https://doi.org/10.1016/j.quascirev.2015.12.00>, 2016

428 Wu, G., Duan, A., Liu, Y., Mao, J., Ren, R., Bao, Q., He, B., Liu, B. and Hu, W.: Tibetan Plateau climate dynamics: recent  
429 research progress and outlook, *Natl. Sci. Rev.*, 2, 100–116, <https://doi.org/10.1093/nsr/nwu045>, 2015

430 Wu, X. C., Li, X. Y., Liu, H. Y., Ciais, P., Li, Y. Q., Xu, C. Y., Babst, F., Guo, W. C., Hao, B. Y., Wang, P., Huang, Y. M.,  
431 Liu, S. M., Tian, Y. H., He, B. and Zhang, C. C.: Uneven winter snow influence on tree growth across temperate China, *Glob.*  
432 *Change Biol.*, 25, 144–154. <https://doi.org/10.1111/gcb.14464>, 2019

433 Yan, L. and Liu, X.: Has climatic warming over the Tibetan Plateau paused or continued in recent years? *J. Earth Ocean Atmos.*  
434 *Sci.*, 1, 13–28, 2014

435 Yang, B., Qin, C., Wang, J., He, M., Melvin, T. M., Osborn, T. J.: A 3,500-year tree-ring record of annual precipitation on the  
436 northeastern Tibetan Plateau, *Proc. Natl. Acad. Sci. U. S. A.*, 111(8), 2903-2908. <https://doi.org/10.1073/pnas.1319238111>,  
437 2014

438 Zhang, Q. B., Evans, M. N., Lyu, L. X.: Moisture dipole over the Tibetan Plateau during the past five and a half centuries, *Nat.*  
439 *Commun.*, 6, 8062. <https://doi.org/10.1038/ncomms9062>, 2015

440 Zhu, H. F., Huang, R., Asad, F., Liang, E. Y., Bräuning, A., Zhang, X. Z., Dawadi, B., Man, W. M., Griessinger, J.: Unexpected  
441 climate variability inferred from a 380-year tree-ring earlywood oxygen isotope record in the Karakoram, Northern Pakistan,  
442 *Clim. Dyn.*, <https://doi.org/10.1007/s00382-021-05736-6>, 2021